Idealised modelling of offshore-forced sea level hot spots and boundary waves along the North American East Coast

Anthony Wise [a,b,*], Jeff A. Polton [a], Chris W. Hughes [b,a], John M. Huthnance [a]

[a] National Oceanography Centre, 6 Brownlow Street, Liverpool L3 5DA, UK
[b] Earth, Ocean & Ecological Sciences, University of Liverpool, 4 Brownlow Street, Liverpool L69 3GP, UK

A B S T R A C T

Hot spots of sea level variability along the North American East Coast have been shown to shift in latitude repeatedly over the past 95 years and connections with a number of forcing phenomena, including the North Atlantic Oscillation (NAO) and Atlantic Meridional Overturning Circulation (AMOC), have been suggested. Using a barotropic 1/12° NEMO model of the North American East Coast (to represent the upper ocean and a homogeneous shelf), we investigate the coastal sea level response to remote sea surface height (SSH) variability along the upper continental slope. Hilbert transform Complex EOF analysis is used to investigate the responses to interannual changes in the strength of the mean winds and an idealised NAO. Variability in the mean winds produces in-phase coastal sea level variability along the entire coastline and is driven by a SSH anomaly in the subpolar gyre. Variability due to the NAO forcing is in phase along the coast south of Cape Hatteras. Interannual coastal sea level variability at a given latitude is found to be driven by off-shore SSH anomalies originating many degrees of latitude (~100s km) further north, and linear barotropic trapped wave theory is used to explain the mechanism. A comparison of the results from an analytical model with those from the numerical model is used to suggest that the boundary wave mechanism is also relevant for understanding the coastal response to interior sea level change over longer time periods. Nonlinear effects are found not to significantly modify the character of the linear solution.

1. Introduction

In recent years a spotlight has been cast over the local and remote drivers of coastal sea level variability along the North American East Coast. Most recently, Volkov et al. (2019) drew attention to a basin scale tripole Sea Surface Height (SSH) pattern of variability linked to the Atlantic Meridional Overturning Circulation (AMOC) and North Atlantic Oscillation (NAO) that was a source of interannual-to-decadal SSH variability along the Southeast Coast of the United States. As in a number of studies looking at these processes, barotropic waves trapped against the western boundary (i.e. the North American East Coast land–sea boundary) are invoked as a possible mechanism for the actual adjustment that occurs between the coast and interior ocean (or elsewhere on the shelf).

The objective of this study is to use an intermediate complexity numerical model, including realistic bathymetry and nonlinear terms, with analysis methods that reveal the propagation of variability, to more thoroughly connect the processes identified by observational studies with the theory of coastally trapped boundary waves. The focus is on the influence of the dynamics of the deep ocean interior on the coast, rather than sea level changes resulting from local winds over shallow water.

In this section we first provide an overview of key results from existing studies that have investigated sea level variability along the North American East Coast on interannual periods. This is followed by a qualitative introduction to how coastal sea level can be connected to interior variability by the mechanism of boundary waves, also referred to as coastally trapped waves. Note that here we use the term *interior* to refer to the interior open ocean, where the effect of sloping bottom topography is small. Furthermore we use the term *shelf* to refer to depths less than about 200 m and *coast* to mean the inner shelf close to the shoreline. The continental slope is generally taken to mean the steeply sloping region of bottom topography connecting the shelf and interior, though we define this more specifically in Section 2 where we describe the numerical model (Section 2.1), experiments (Section 2.2) and the method of analysis (Section 2.3). Following this we present our results and discuss them in relation to the results of previous studies (Section 3.2), boundary wave theory (which we explain with a specific example, Section 3.3) and nonlinear effects (Section 3.4). Finally, we discuss our results in a broader context and then conclude with a summary.

* Corresponding author at: National Oceanography Centre, 6 Brownlow Street, Liverpool L3 5DA, UK.
   E-mail address: anwise@noc.ac.uk (A. Wise).

1.1. Sea level variability along the North American East Coast

Coastal "hot spots" of accelerated sea level rise and variability have the potential to add to any global mean sea level rise, making the adjacent coast vulnerable to shorter time scale events that can cause flooding, for example storm surges. The mechanisms that govern these hot spots are therefore of particular interest. Using observations, Sallenger et al. (2012) identified a hot spot along 1000 km of the North American coastline north of Cape Hatteras, where the rate of increase of sea level rise was of order 3–4 times larger than the global average during 1980–2009. While it remains debated, they suggested the sea level rise might be associated with a slowdown of the AMOC. In addition to the AMOC, a number of processes, both local and remote, have been investigated as drivers of this hot spot, and assigning causality between sea level anomalies and forcing, more generally, has been shown to be complex due to the coupling of driving phenomena. Kenigson et al. (2018) suggest that changes in the local wind stress (particularly alongshore), linked to the NAO, are strongly related with sea level anomalies north of Cape Hatteras. Similarly, Piecuch et al. (2016) show annual coastal sea level changes north of Cape Hatteras to be driven by wind stress over the continental shelf and slope, and highlight the apparent dominance of barotropic dynamics in the adjustment of coastal sea level to forcing. Furthermore, the anticorrelation between coastal sea level north of the Cape and overturning circulation at 26N is suggested by Piecuch et al. (2019) not to be causal, but instead driven by temporally coherent, but different, forcing mechanisms. In the case of the former, local alongshore wind and air surface pressure are responsible, and in the latter, zonal wind stress along 26N is responsible — though they note the potential role of large-scale atmospheric modes of variation linking them, such as the NAO. In terms of remote drivers, over a 50 year period of observations (1965–2014) Frederikse et al. (2017) found a strong correlation between coastal sea level north of the Cape and decadal steric variability in the Subpolar Gyre. The steric height showed an upward sea level trend and acceleration, which is also found along the coast. They suggest the variability likely originates in the Labrador Sea, from where it propagates southward. The linkage between coastal sea level and the Labrador Sea is also noted by Andres et al. (2013), with a similar correlation map, though they note the mechanism of propagation onto the shelf is not clear.

Sea level variability along the North American East Coast is subject to regional differences north and south of Cape Hatteras, where the Gulf Stream separates from the western boundary. This has led to investigations into the connection between the Gulf Stream and coastal sea level. In particular Ezer et al. (2013) and Ezer (2019) suggest that changes in the strength of the Gulf Stream and its position relative to the Middle Atlantic Bight, north of Cape Hatteras, affects sea level gradients. They conclude that a strong Gulf Stream leads to lower coastal sea level in the Middle Atlantic Bight, while the effect is reduced south of the Cape.

Variability in the strength of the Gulf Stream can itself, of course, be a consequence of large-scale forcing variability. Valle-Levinson et al. (2017) show that between 2011 and 2015, sea level rise actually decelerated north of Cape Hatteras, while accelerating to 3 times the global mean south of the Cape — the latter phenomenon also being reported by Park and Sweet (2015). Valle-Levinson et al. (2017) show this sea level rise hot spot to be active over the past 95 years with a shifting latitude. They suggest that the existence of the hot spot is conditional upon the cumulative effects of El Niño and that the latitudinal position depends on the cumulative effects of the NAO. The acceleration of sea level rise south of the Cape has also been attributed to a 0.2°C per year warming of the Florida Current and the deceleration north of the Cape to a combination of increased atmospheric surface pressure, changing wind patterns and cooling (Domingues et al., 2018). Volkov et al. (2019) suggest that sea level south of the Cape is largely driven by large-scale meridional heat transport influenced by the AMOC. Stronger mean heat transport by the Florida Current leads to higher thermosteric

sea level in the interior ocean at mid latitudes, which is then coherent with coastal sea level, and they show the very large-scale first mode of variability of SSH, steric and thermosteric sea levels to have a similar tripole spatial pattern. They also point to the large-scale atmospheric forcing, with a positive NAO also leading to higher interior sea level across the same latitude band. The NAO+ shifts the zero wind stress-curl line northward and increases its zonal tilt, i.e. the eastern portion of the zero wind stress-curl is shifted farther northward. The NAO- results in a more zonal zero wind stress-curl. This feature of the NAO in terms of ocean circulation has been discussed by Marshall et al. (2001). In terms of sea level, the resulting increase or decrease in interior SSH near Cape Hatteras appears to influence the SSH on the shelf along the Florida coastline. Remote forcing from the interior ocean has also been put forward as an explanation for large interannual to decadal variability in the amplitude of the sea level annual cycle south of Cape Hatteras (Calafat et al., 2018). They suggest that larger amplitudes in the annual cycle, coherent along much of the coast from Cape Hatteras into the Gulf of Mexico, are the result of density anomalies in the interior ocean travelling westward towards the western boundary. They note that larger annual cycle amplitudes correspond with larger annual upper mid-ocean transport, which would be explained by a larger pressure gradient between eastern and western boundaries of the Atlantic. This latter point clearly brings into focus the connection between western boundary sea level and the AMOC – discussed in detail by Bingham and Hughes (2009) and Little et al. (2019) – with consequences for meridional heat transport (Zhai et al., 2011), and thereby also the climate.

Clearly there are a number of forcing phenomena that are correlated with coastal sea level variability; however, in order to explain the spatial distribution of coastal sea level variability we must also consider the actual process of adjustment between the coast and interior ocean. Linear theory with idealised geometry and bathymetry suggests that western boundary sea level is determined by what occurs poleward of the point being considered (Wise et al., 2018, 2020; Minobe et al., 2017), but this neglects any possible role of advection by a boundary current. This work takes the next step by considering realistic bathymetry, and allowing nonlinear terms so that advection of potential vorticity is accounted for.

1.2. Boundary waves

Because the western boundary acts like a wall, a flow approaching the coast must either diverge in the along-shore direction or sink to become balanced by an offshore bottom Ekman flow, implying that the dynamics at the coast are not as they are in the interior ocean. This has important consequences for how sea level variability is spatially distributed along the coastline and draws attention to the role of the continental slope in separating the shelf from the interior ocean. While SSH anomalies can spread relatively slowly via advection by the current, here we look at the quicker mechanism of signal propagation by waves trapped to the coast (boundary) (Huthnance, 1975, 1978).

Huthnance (1987), Chapman and Brink (1987) and Huthnance (2004) show that in idealised experiments with stratification, forcing in the interior ocean due to wind stress or density gradients elicits an essentially barotropic response along the shelf, which propagates over long distances, with the boundary on the right in the northern hemisphere. These waves are trapped in the sense that they decay in amplitude away from the boundary. For eastern boundaries, Clarke and Van Gorder (1994) show that at typical El Niño-Southern Oscillation (ENSO) frequencies, on-shelf sea level (sea level on the shelf) signals travel poleward with a reduction in amplitude as latitude increases. Using isopycnal models validated with altimetry, Roussenov et al. (2008) find that changes in high-latitude forcing are communicated along the western North Atlantic continental slope by boundary waves over several thousand kilometres. The result is coherent signals in SSH and bottom pressure variability over large distances — see also Hughes and Meredith (2006) and Hughes et al. (2018).

The body of literature investigating coastally trapped waves (CTW) in various settings is extensive, see Hughes et al. (2019), Brink (1991), Huthnance et al. (1986) and Mysak (1980) for reviews. Here, by assuming that the response on the shelf and upper slope is dominated by barotropic dynamics, as studies noted above suggest, we focus specifically on barotropic waves, which can also be thought of as waves in a homogeneous upper layer of the ocean that is grounded on the sea floor between the upper slope and coast i.e. its lower surface is in contact with the shelf and upper slope. Offshore, the layer represents only the upper portion of the water column, and is considered to have a motionless, rigid ocean beneath, which does not exchange any fluid with the upper layer. This simplification allows us to model the barotropic adjustment at the coast to an interior SSH anomaly, regardless of which specific forcing phenomenon produced it, i.e. wind or density induced SSH anomaly. We simply relate coastal sea level to the interior sea level (remote forcing). For example, fluctuations in wind stress in the interior ocean produce a SSH anomaly in the interior ocean that elicits a response on the shelf and slope (remote forcing).

For annual to decadal forcing periods, Marshall and Johnson (2013) showed for the first baroclinic mode wave, and Wise et al. (2020) showed for barotropic topographic waves, that interior SSH anomalies (possibly carried westward by long Rossby waves) modify the amplitude (and speed) of southward propagating boundary waves (generated by local and remote forcing farther northward). As the southward propagating boundary waves dissipate energy due to friction, they reduce in amplitude and the incident long Rossby waves from the interior modify the amplitude of the boundary waves to a greater extent, thereby allowing greater penetration of interior SSH variability. Importantly, the rate of dissipation has been shown to depend on a number of factors: steepness and width of the bottom topography, friction parameter, as well as latitude (Wise et al., 2020, 2018; Huthnance, 2004; Chapman and Brink, 1987; Brink and Allen, 1978). This theory will be described in more detail in Section 3.3. Note that while we do not explicitly cover the case of local forcing on the shelf, on-shelf alongshore wind stress forcing also produces topographic waves that propagate with the coast on the right.

2. Model and analysis method

2.1. Model setup

The model is based on a 2d configuration (Polton et al., 2020) of the NEMO 4.0 General Ocean Circulation model (Gurvan Madec and NEMO System Team, 2019) that we have modified to create a barotropic North Atlantic western boundary. The model has one active layer using a terrain following s-coordinate, and the horizontal grid is a 1/12 of a degree grid using the NEMO ORCA_R12 grid. While the bottom topography at the western boundary is realistic – we use the 15 arc-second GEBCO Compilation Group (2019) gridded data set – we modify it in two ways. Firstly, we set the maximum depth for the entire domain to a constant $H_c = 500$ m, i.e. any depth $H(x, y)$ greater than H_c is set equal to H_c. This allows us to represent an idealised upper ocean layer between the upper slope and coast. As a result, throughout the text, the *slope* refers to the regions where the bathymetric depth is between 200 and 500 m. Consequently, the interior upper ocean layer is considered to begin at the 500 m depth contour. Recall, that we define the shelf region as bathymetric depth less than 200 m and the coast to be the very inner shelf region. It should be noted here that 500 m will not be the ideal upper layer thickness for all latitudes. Wise et al. (2018) suggest that for an idealised linear barotropic ocean, a thinner upper ocean layer thickness will increase the penetration of sea level anomalies from the interior to the coast, and is equivalent to increasing the bottom friction parameter or decreasing the width of the shelf.

A second modification made to the bathymetry is a truncation to the eastern extent of the domain to roughly follow the Mid Atlantic Ridge, which retains an adequate interior ocean for subpolar and subtropical gyres to form and set up the interior SSH.

Table 1
Values of the parameters used in the model: max depth H_c, friction coefficient on shelf and slope C_D^s, friction coefficient over flat bottom interior ocean region C_D^{in}, bilaplacian horizontal diffusion coefficient B_h and the partial slip parameter value (where 0 is free slip and 2 is no slip).

H_c	C_D^s	C_D^{in}	B_h	Partial slip parameter
500 m	2.3×10^{-3}	4×10^{-4}	-5×10^9 m^4 s^{-1}	1

The lateral boundaries are closed except for the northern and southern boundaries, which have Flather (1994) radiation conditions imposed on the velocity normal to the boundary, allowing gravity waves to exit the domain (external field variables are taken to be zero). The purpose of the Flather condition is to minimise any artificial leakage of the interior ocean signal onto the shelf close to the boundary, however we do also consider the case where the northern and southern boundaries are closed. For land boundaries partial slip is imposed.

For bottom friction, which is non-linear, it is sensible to assume that there is a reduced frictional effect on the upper layer of the flow in the interior ocean, and we therefore use two different friction coefficients; one for the shelf and slope C_D^S, and another smaller value, C_D^{in}, for greater depths (i.e. where $H = H_c$). The main effect of this is to create a more realistic boundary current, since a large friction parameter in the interior ocean was found to create an unrealistically wide boundary layer in preliminary experiments (to some extent the quadratic friction formulation used will also reduce bottom friction effects in the deeper open ocean). Ultimately our goal is to create a realistic interior SSH to relate to the on-shelf SSH. Finally, the model is set up to use a lateral bilaplacian diffusive operator and a free surface. All parameter values are listed in Table 1.

2.2. Forcing

Forcing of the model is provided exclusively via an idealised zonal wind stress, τ_u. All other forcing mechanisms are turned off. As previously noted, from an analysis point of view, it is unimportant how the interior ocean SSH is set up; however, using wind stress allows us to maintain extremely simple boundary conditions while selecting a wind stress magnitude that results in quite realistic SSH gradients. The wind stress magnitude applied is unrealistically large, i.e. approximately double observed values; however, this is also physically reasonable given the reduced domain width.

The model experiments have two forcing stages, a "spin-up" stage, and a stage where the wind stress changes in time and space. During the spin-up, a quasi steady state is established using a time independent zonal wind stress, which we consider as the time mean wind stress $\tau_u^M(x, y)$, as shown in Fig. 1a. The spatial structure of this wind stress forcing pattern is chosen to be representative of the long period time-mean zonal wind stress, e.g. see Hellerman and Rosenstein (1983). Note that a key feature of the wind pattern is the intersection of the zero wind stress curl contour with the western boundary, and also its basin scale characteristics, i.e. the zero curl line (where τ_u is maximal or minimal) is not zonal. In Fig. 1a the zero wind stress curl corresponds to the contours emanating from 35N and 20N. The latitude of the zero wind stress curl, relative to Cape Hatteras, plays an important role in how the Gulf Stream separates from the boundary and this has been discussed in detail for a barotropic ocean e.g. Dengo (1993), Munday and Marshall (2005) and for more complex settings e.g. Chassignet and Marshall (2008) and Bryan et al. (2007). In terms of the interior SSH, this is important for creating a realistic "step-up" in SSH where the Gulf Stream separates. Using a spin-up period of 3 years, Fig. 2a shows the model SSH across the entire domain, and Fig. 2b shows the model SSH along the 800 m and 40 m depth contours as well as the Mean Dynamic Sea Level (MDSL) derived from altimetry along the same contours — note that the contours are denoted in Fig. 2a. The MDSL is the 22-year mean (1993–2014 inclusive) from AVISO (the Ssalto/Duacs,
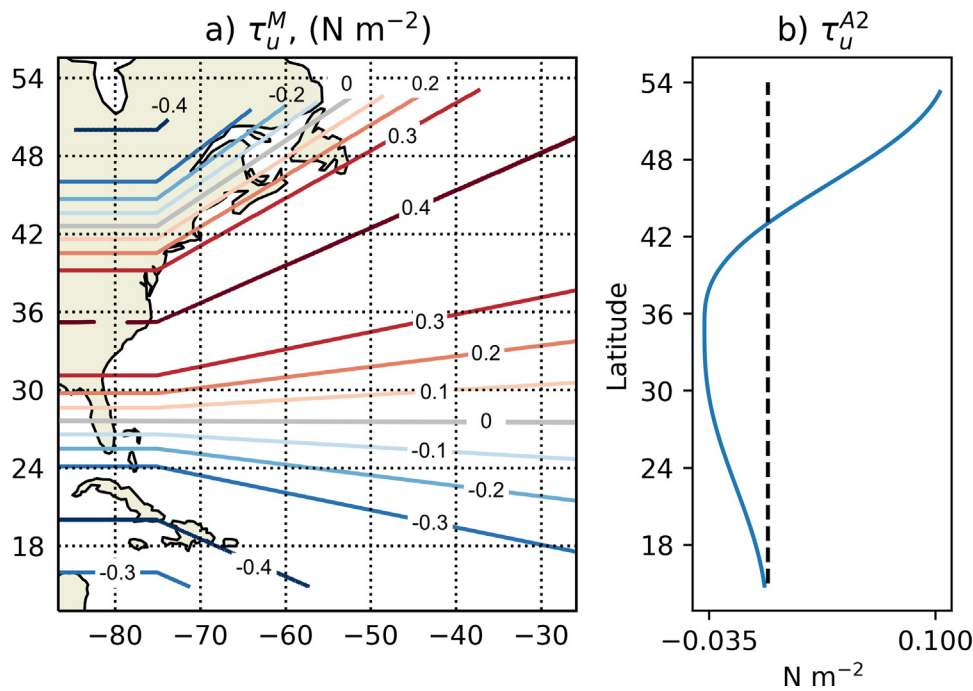
Fig. 1. (a) Contours of τ_u^M: the steady, purely zonal wind stress applied to establish a mean circulation. (b) The additional zonal wind stress τ_u^{A2} which is applied at all deep water longitudes with a time-dependent amplitude, to simulate NAO variations, following Zhai et al. (2014).

delayed mode, gridded absolute dynamic topography product using all available satellites). Given the relatively simple nature of the model (idealised forcing and vertical structure), it is surprising how well the model captures the observed SSH. The main differences to note are that the model Gulf Stream separates slightly too far southward and some on-shelf processes are obviously missing. The sub polar SSH low is also slightly under represented, which is probably due to the missing eddy-driven recirculation gyre just north of the Gulf Stream, between approximately 36N and 41N (See Fig 3 of Liu et al. (2018)).

Following the 'spin-up', a wind stress anomaly $\tau_u^A(x, y, t)$ that varies in space and time is added to the mean field

$$\tau_u(x, y, t) = \tau_u^M(x, y) + \tau_u^A(x, y, t). \tag{1}$$

To isolate the relationship between interior and coastal SSH, the wind stress anomaly is damped close to the continental slope of the North American mainland and set to zero on the shelf and slope. This ensures that variability on the shelf and slope is due to interior ocean dynamics only. Defining the wind stress in this way does have the drawback of introducing an artificial wind stress curl between the interior and coast; however, with adequate damping, i.e. avoiding large $\partial \tau_u / \partial y$, this contribution is found to only moderately affect the zonal integral of the wind stress curl (not shown) and does not materially affect the results and discussion presented. Specifically, the wind stress anomaly, τ_u^A, is set to zero on the shelf and slope of the North American mainland (i.e. not the various islands in the domain) and a linear ramp up is applied over approximately 2 degrees of latitude from the foot of the upper continental slope at the 500 m isobath.

The wind stress anomaly is defined to induce two general effects on the interior SSH, representative of the interior ocean variability suggested by observational studies. Firstly, we wish to fluctuate the magnitude of the SSH north and south of the Gulf Stream separation latitude. This is achieved by simply adding a wind stress contribution, $\tau_u^{A1}(x, y, t)$, that modulates the mean wind stress amplitude in time, but with the same spatial pattern as the mean, i.e. as shown in Fig. 1a. This contribution to the anomaly is periodic with a period of 4 years and amplitude 0.1 N m^{-2} — the mean field amplitude is 0.4 N m^{-2}. This forcing pattern is referred to in the remainder of the text as the Mean Forcing Pattern. In addition, we wish to fluctuate in time the spatial

structure of the interior SSH. This is achieved by adding another wind stress contribution, $\tau_u^{A2}(y, t)$, which is zonally uniform (except for the damping) and differs from the mean field in its latitudinal structure, see Fig. 1b. Again, this contribution to the anomaly is periodic, but with only a 2 year period. Note that $\tau_u^{A2}(y, t)$ is based on the wind anomaly due to the NAO. Specifically, we have approximately represented the meridional NAO profile used by Zhai et al. (2014), where they have regressed monthly reanalysis zonal wind stress onto the NAO index for the period 1950–2010 and then zonally averaged (i.e. multiplying this wind stress by the monthly NAO index gives a zonal-mean wind stress anomaly that fluctuates in time with the NAO index). We will refer to this forcing pattern as the NAO Forcing Pattern.

In the above cases the SSH gradients result from the mounding and depression of SSH due to wind driven convergence and divergence. The currents in and out of the western boundary, which are associated with the SSH gradients, are therefore strengthened and weakened as the gradients increase and decrease respectively. For example, Valle-Levinson et al. (2017) propose that La Niña and El Niño climate patterns result in a modulation of the wind stress magnitudes in the North Atlantic via the Pacific-North American Teleconnection, producing an increase and decrease, respectively, of volume transport into the western boundary, which they suggest is connected to a coherent sea level rise and fall along the US east coast. Our Mean Forcing Pattern is similarly a modulation of mean wind stress magnitude. Our NAO Forcing Pattern effectively adds a modulation in wind stress which is shifted northward relative to the mean pattern.

It is important to appreciate that such interior sea level gradients can also be the result of thermal expansion and contraction of the water column. For example, south of Cape Hatteras, sea level gradients can increase due to variability in warming of the Florida current (Domingues et al., 2018) or due to variability in the volume transport of the Florida current, for example, which can advect temperature and generate meridional heat transport (Volkov et al., 2019). North of Cape Hatteras, similar steric variability and sea level gradients can result from temperature and salinity anomalies in the southern subpolar gyre (Frederikse et al., 2017). The coupling between heat and salt fluxes, variations in circulation such as the AMOC and large-scale atmospheric patterns such as the NAO is complex (see for example Volkov et al. (2019)), and to
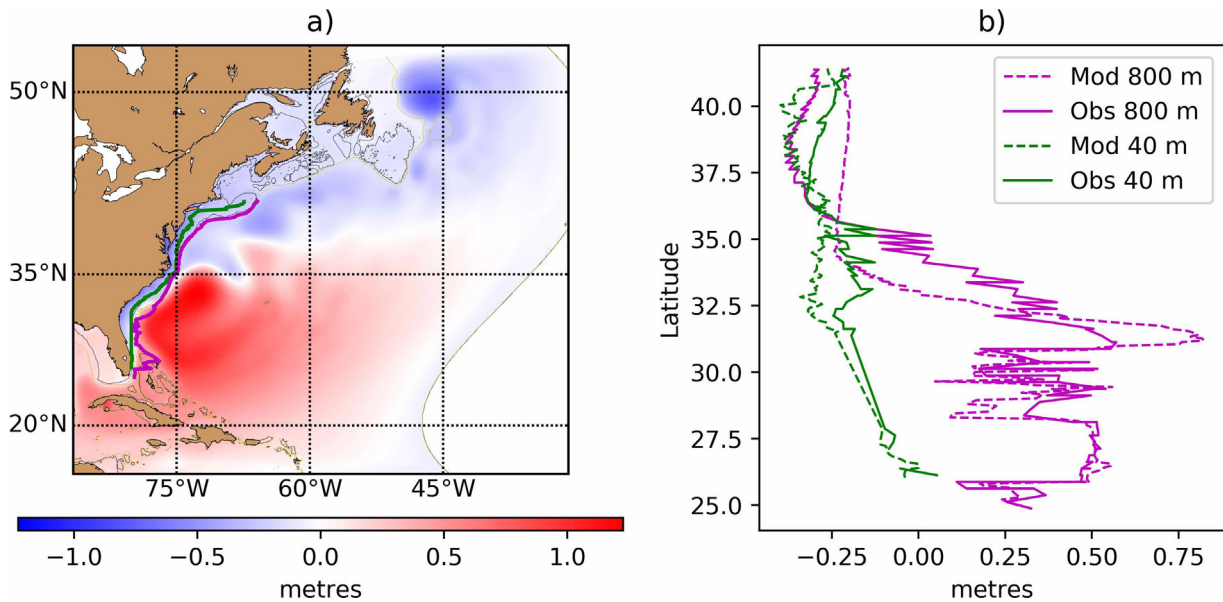
Fig. 2. (a) Quasi-steady state Sea Surface Height (SSH) from the model after a three-year spin up. (b) Model Sea Surface Height (Mod) after the 3-year spin up and satellite derived Mean Dynamic Sea Level (MDSL) (Obs) along the 40 and 800 metre depth contours as a function of latitude. The contours are shown in panel (a). The difference between the means (spatial mean taken over latitude) of the 800 m SSH and 800 m MDSL has been removed from the 40 m and 800 m MDSL.

restate, while the forcing phenomena are clearly of importance, we are focusing on the relationship between an interior SSH and the on-shelf SSH.

In order to efficiently use computer time we apply both fluctuating fields simultaneously (over a 4 year model run) and separate out the responses in post processing. The fluctuating wind stress anomaly is therefore defined as

$$\tau_u^A(x,y,t) = D(x,y)\left[\tau_u^{A1}(x,y,t) + \tau_u^{A2}(y,t)\right], \tag{2}$$

where $D(x,y)$ is the damping. This fluctuating forcing is used to set up SSH variability that represents the interior SSH variability described in the various observational studies discussed in the introduction.

2.3. Data analysis

To determine the connection between the interior ocean and coastal sea level, we apply a Hilbert transformed Complex Empirical Orthogonal Function (CEOF) analysis to the model SSH output. Unlike with correlation maps or standard EOFs, this approach allows us to investigate the spatial and temporal phase and amplitude of the domain-wide response.

A full review of the method is described by Hannachi et al. (2007), here we give a brief overview of the method. For the SSH field anomaly $\boldsymbol{\eta}_t = (\eta_{t,1}, \eta_{t,2}, \ldots, \eta_{t,m})^T$, where m is the total number of grid points and $t = 1, 2, \ldots, n$ is the time index, the complex field is

$$\xi_t = \eta_t + i\mathcal{H}(\eta_t), \tag{3}$$

where $\mathcal{H}(\cdot)$ denotes the Hilbert transform operator. This results in an imaginary part of the time series in which each Fourier component is the same as for the real part, but with a 90 degree phase shift. The EOFs of $(\xi_1, \xi_2, \ldots, \xi_n)$ are complex, and the spatial amplitude of the kth CEOF, $\boldsymbol{p}_k$, is given by

$$a_k = |\boldsymbol{p}_k|, \tag{4}$$

where $|\cdot|$ denotes the component-wise absolute values of $\boldsymbol{p}_k$. The spatial phase of the kth CEOF is then

$$\theta_k = \arg(\boldsymbol{p}_k), \tag{5}$$

where $\arg(\cdot)$ denotes the component-wise arguments of $\boldsymbol{p}_k$. Similarly, the temporal amplitude and phase are obtained from the Complex

Principal Components (CPC), $\boldsymbol{q}$, such that the temporal amplitude of the kth CPC is

$$b_k = |\boldsymbol{q}_k|, \tag{6}$$

and the kth temporal phase is

$$\boldsymbol{\phi}_k = \arg(\boldsymbol{q}_k). \tag{7}$$

The variability described by each kth mode can therefore be written as

$$a(x,y)b(t)e^{i[\theta(x,y)+\phi(t)]}, \tag{8}$$

with a summation of all modes returning the original signal (subscript k is implicit). By design virtually all variability in our experiments is attributable to the two wind stress forcing patterns that we have imposed. As a result, the temporal amplitude and temporal phase of the two modes of variability that the CEOF analysis finds are simply close representations of the forcing patterns' temporal evolution. For example the temporal phases represent the 4 yr and 2 yr periods of the two forcing patterns. As a result we do not present the resulting temporal amplitude and phase plots but instead normalise the spatial amplitudes by maximum temporal amplitude and present the spatial phases so that $-90°$ is in phase with the wind forcing and $90°$ is out of phase with the wind forcing.

The reason that CEOFs have been used is that while the spatial amplitude $a(x,y)$ is modulated in time by $b(t)$, the spatial phase gives a sense of how anomalies propagate in space given the frequency of the wind forcing, i.e. from (8), the temporal phase $\phi(t) \approx \omega t$, where ω is the frequency of the wind forcing. Spatial propagation can then be qualitatively captured because the spatial derivative of $\theta(x,y)$ gives a local wavenumber.

3. Results and discussion

In this section we will present and discuss the CEOFs in context with the results from existing observational studies and boundary wave theory.

3.1. CEOFs & modes of variability

The CEOF analysis of the model SSH output by design reveals two dominant modes of variability, accounting for ~95% of the variability,
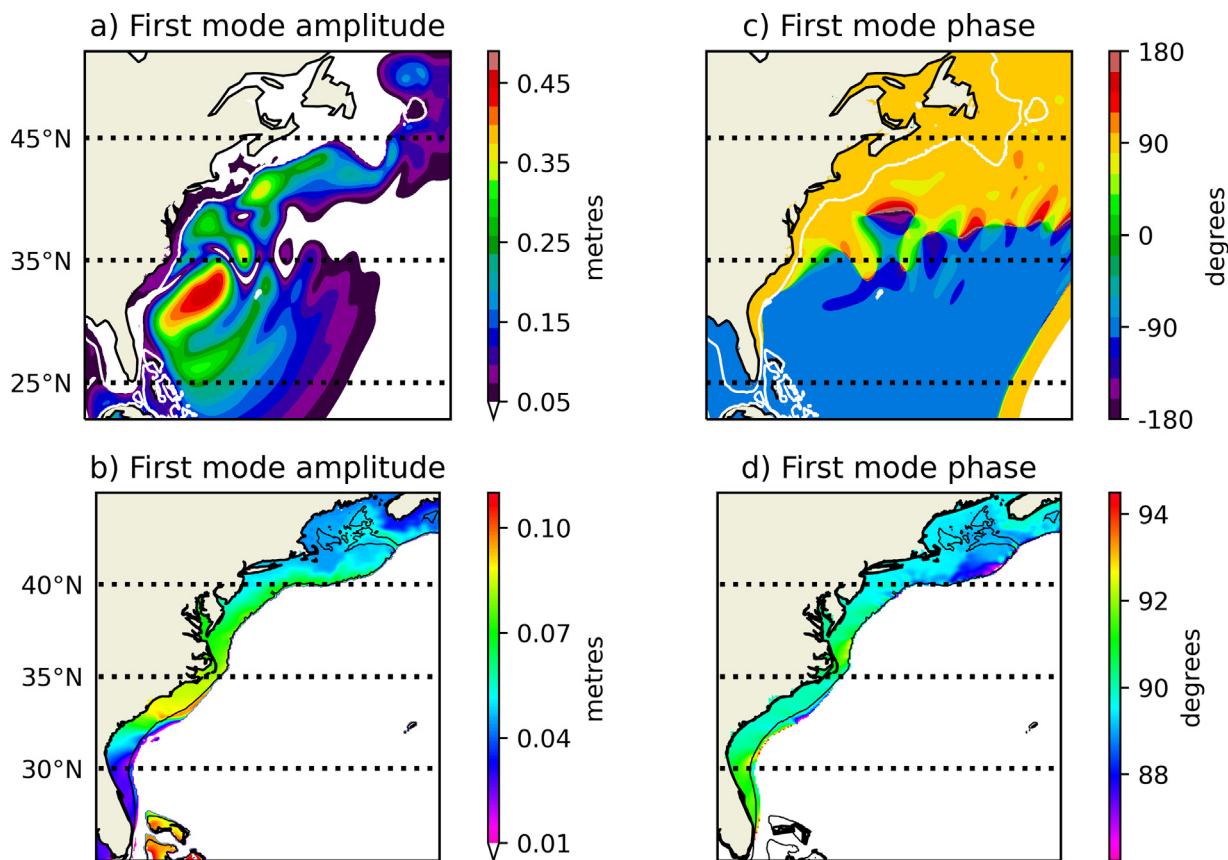
Fig. 3. Panels (a) and (c) are the spatial amplitude and phase of the Complex EOF of model Sea Surface Height corresponding to the Mean Pattern forcing. Only the interior ocean has been forced with the zonal wind stress anomaly. Panels (b) and (d) are the same but focused on the shelf and slope using a high resolution colourmap. The white contour is the 500 m isobath and the black contour is the 200 m isobath.

with the modes associated with the two forcing patterns i.e. the Mean Forcing Pattern and the NAO Forcing Pattern. Note that the relative variance explained by each could be somewhat misleading, given that it will depend on the amplitudes we have chosen for the two wind stress contributions. With that said, the two different wind stress amplitudes are comparable and it is interesting to note the similarity of the variance explained with that found for the two dominant EOF modes by Valle-Levinson et al. (2017), which were suggested to be related to ENSO and the NAO.

Panels a and c in Fig. 3 show the spatial amplitude and phase, respectively, of the Mean Pattern (τ_u^{A1}) CEOF, which accounts for 71% of the variability (note that panels b and d show the amplitude and phase on the shelf and slope in finer detail and will be considered in Section 3.3 for the discussion on the propagation of variability). Panel a shows the amplitude of SSH variability in the interior ocean (white contour denotes 500 m isobath) resulting from strengthening and weakening of the subpolar and subtropical gyres as the magnitude of the zonal windstress increases and decreases. Along the coast there is clear leakage of interior SSH variability onto the shelf, with amplitudes substantially reduced. The largest coastal variability is seen between 32N and 38N, around Cape Hatteras. Panel c shows the coastal variability along the entire North American east coast, as far south as 25N, to be coherent (relative to the long 4-year period of the mode), implying rapid propagation. Generally speaking, this coastal signal is in phase with the interior signal north of 37N and mostly out of phase with the interior signal south of 37N (although the signal immediately offshore of the slope is also in phase with the shelf extending to about 33N). The Mean Pattern mode coastal SSH anomaly is therefore of reduced magnitude compared to the interior (it is attenuated) and there is a southward displacement, i.e. the anomaly at the coast appears to be farther south than in the interior.

Panels a and c in Fig. 4 show the spatial amplitude and phase for the NAO Pattern (τ_u^{A2}) CEOF, accounting for 22% of the variability. Together they show NAO+ (NAO−) forcing a positive (negative) SSH anomaly across much of the interior, which penetrates in-phase onto the shelf, most notably south of 33N (the amplitude of shelf variability north of 33N is very small). The on-shelf variability differs from the Mean Pattern in that it is entirely in-phase with the interior.

With no direct forcing on the shelf and slope, the immediate implication from the two modes of variability is that phenomena increasing the interior SSH will drive a smaller increase in coastal SSH that is displaced southward along the coast relative to the interior signal. In the Mean Pattern mode case, the amplitude initially grows in the southward direction, with the increasing influence of the subpolar gyre, then it starts to decrease as the out-of-phase subtropical gyre influence penetrates. In the NAO Pattern mode case, interior sea level is in phase everywhere, so the coastal sea level signal keeps increasing all the way to the tip of Florida. As will be discussed in the following two subsections, this is consistent with observational studies and linear wave theory.

Before discussing observations, it should be noted that the radiative boundary conditions at the northern and southern boundaries of the domain can have an impact on the character of the modes of variability. For example, a large portion of the variability in the NAO Pattern mode (Fig. 4a and b) is in phase, which implies that the majority of the surface elevation tends to rise and fall coherently across the domain. This suggests that mass is not conserved and implies that the Flather boundary conditions are playing a large role in leaking mass in and out of the domain. In the real ocean, mass would be able to spread north and south of the domain being modelled, as occurs here, but here the dynamics that are occurring in these unmodelled regions is being lost.
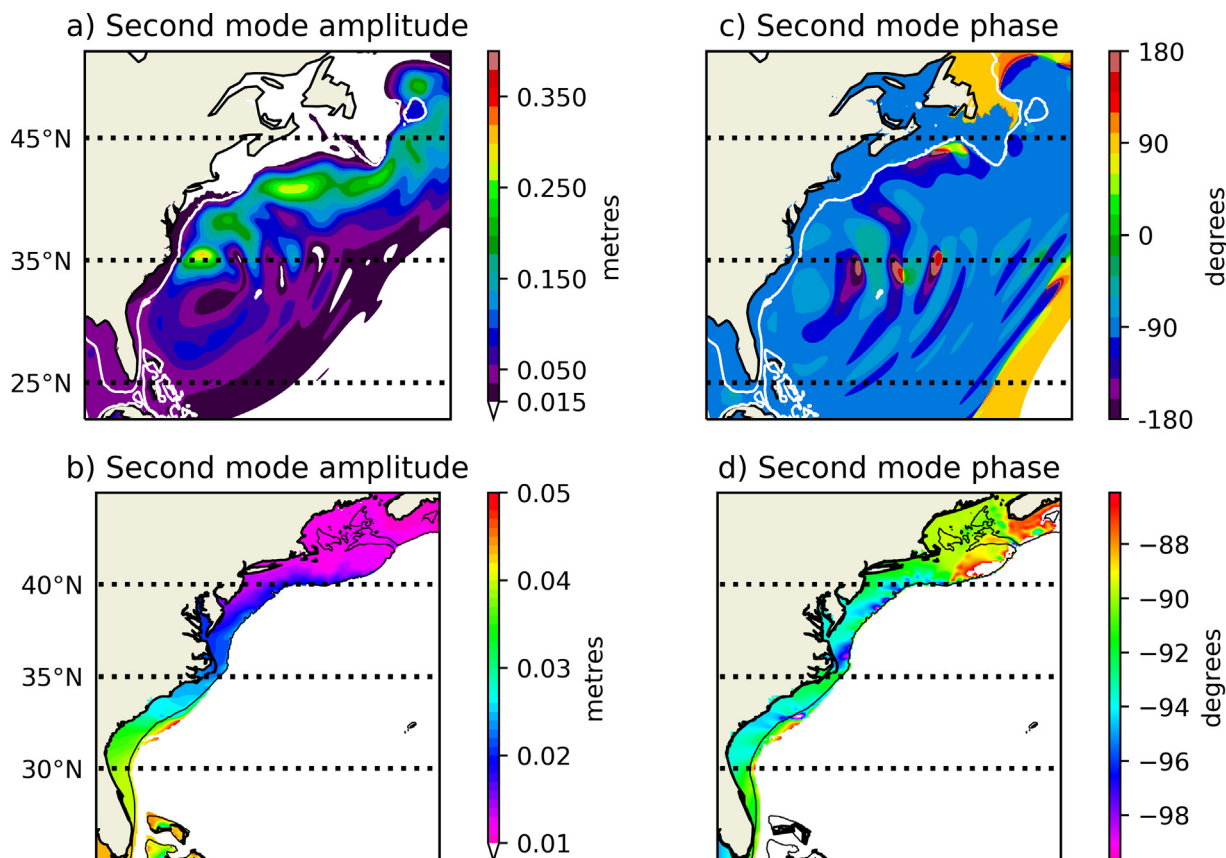
Fig. 4. Panels (a) and (c) are the spatial amplitude and phase of the Complex EOF of model Sea Surface Height corresponding to the NAO forcing. Only the interior ocean has been forced with the zonal wind stress anomaly. Panels (b) and (d) are the same but focused on the shelf and slope with a high resolution colourmap. The white contour is the 500 m isobath and the black contour is the 200 m isobath.

To demonstrate this issue more clearly, Figs. 5 and 6 show the same experiment with closed northern and southern boundaries. It is clear from panels a and c in Fig. 6 that the NAO Pattern mode of variability is indeed strongly influenced by the boundary conditions, with the on-shelf response significantly altered. This can be explained as follows. With mass unable to leak from the domain, the surface elevation in the northern and southern portions of the domain is out of phase with the central band of the domain due to conservation. This does not occur in the Flather experiment. This ultimately results in a very different on-shelf response, because variability on the shelf is strongly controlled by variability occurring at higher latitudes than the point of interest on the shelf. In fact the contrast between the two experiments highlights this point quite clearly and the mechanism behind this important result is discussed in more detail in Section 3.3.

Clearly the choice of boundary conditions is an important concern. Here we suspect that the reality is somewhere between the two cases (Flather and Closed). This is because some spreading of mass northward and southward of the domain should be expected in reality, and this would be compensated for at other locations in the interior ocean that have also not been included in the domain (but crucially that are not necessarily adjacent to the continental slope, as is the case in the Closed experiment).

3.2. Consistency with observational studies

Most strikingly, the results of the NAO Pattern mode are consistent with coherent variability on the shelf, south of Cape Hatteras, being forced remotely. This can occur by warming/cooling of the Florida current, as found by Domingues et al. (2018), Volkov et al. (2019), and by the NAO (Valle-Levinson et al., 2017; Volkov et al., 2019). Similarly, interior ocean anomalies have been shown to modulate the amplitude

of the sea level annual cycle south of the Cape (Calafat et al., 2018). The Mean Pattern mode is also consistent with the correlation maps in Frederikse et al. (2017) and Andres et al. (2013) depicting coherence between the coastal sea level variability north of Cape Hatteras and the interior sea level farther northward — though their correlation maps do not show coherence extending significantly south of Cape Hatteras as found here. Perhaps most interestingly, the EOF modes of coastal 5 yr rates of sea level change depicted in figure 3 of Valle-Levinson et al. (2017) bear a remarkable resemblance to the two modes presented here. They show their first mode as being responsible for in-phase variability along the entire coastline whereas their second mode is responsible for variability along the entire coastline, but in anti-phase, roughly about Cape Hatteras. The combination of the two modes results in a hot spot which is highly mobile latitudinally. Our results support the idea that multiple modes of variability could be important for understanding North American east coast hot spots. An interpretation of observations together with our modelling results are as follows:

- A mode of variability acts coherently and in phase along the coastal zones both north and south of Cape Hatteras; this mode is driven by a modulation of interior SSH gradients north of Cape Hatteras, due potentially either to strengthening of the westerlies or steric variability in the southern sub-polar gyre Frederikse et al. (2017).
- A second mode of variability also acts coherently along the entire coastline. This can be related to the effect of the NAO+(−) (and in reality also to warming (cooling) of the Florida current) creating off-shelf SSH highs (lows) in the sub tropical band of the ocean and on-shelf highs (lows) south of Cape Hatteras. While this mode acts coherently along the entire shelf, observational studies
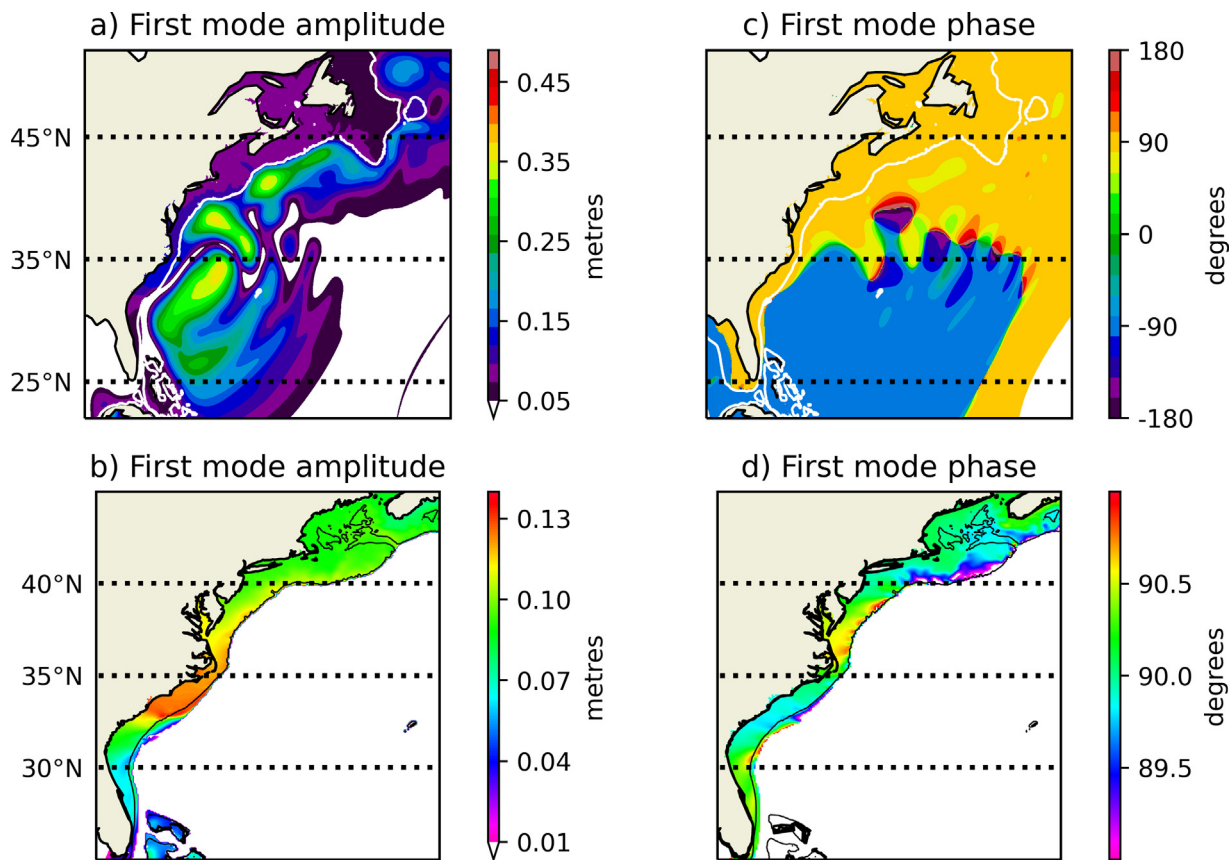
Fig. 5. As in Fig. 3 but for closed northern and southern boundaries.
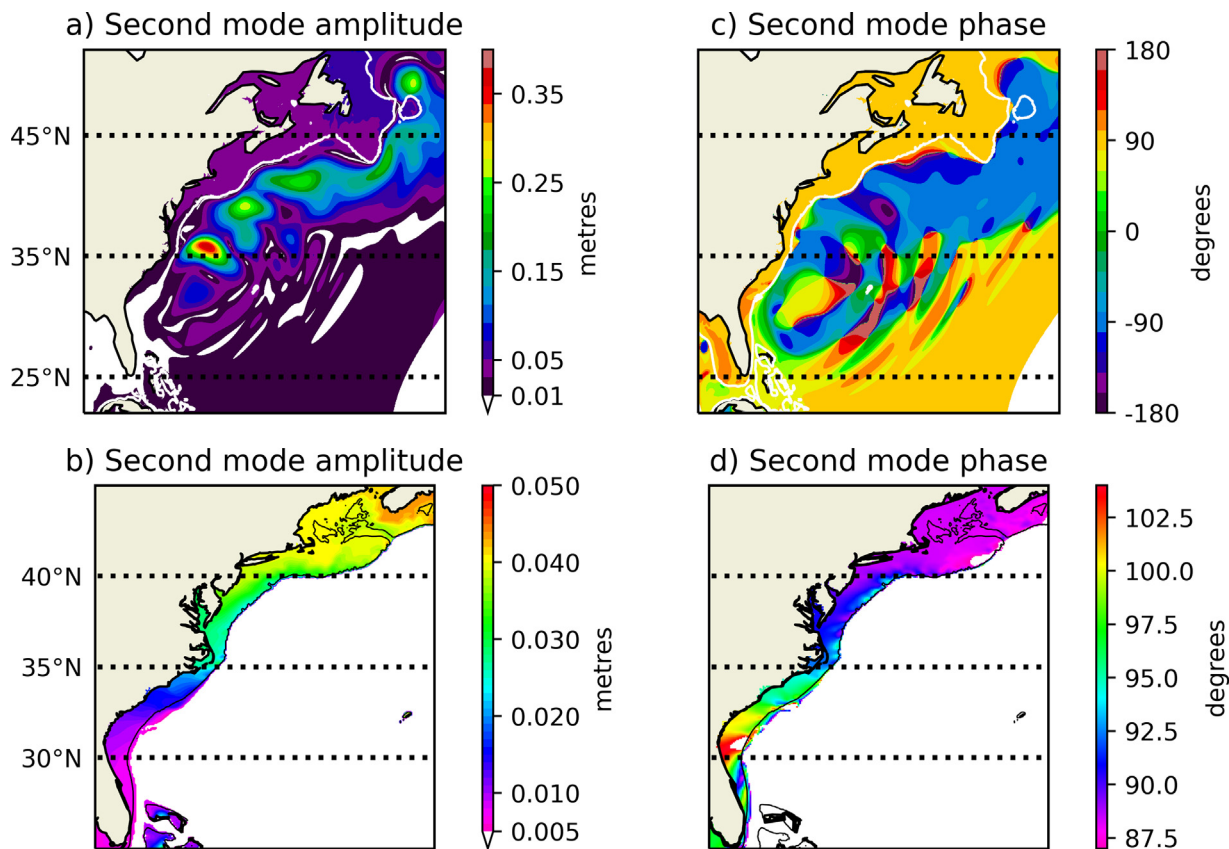

Fig. 6. As in Fig. 4 but for closed northern and southern boundaries.

discussed in the introduction, i.e. Piecuch et al. (2019), suggest that the NAO can also modulate on-shelf winds north of Cape Hatteras, which we have not included, that could modify the phase of the response north of the Cape.

3.3. Relating hot spots to boundary waves

The coherence of the signal along the shelf, despite the absence of direct forcing on the shelf, suggests that interior variability generates a long barotropic trapped wave response at the boundary, which rapidly transmits SSH information southward along the coast.

To understand the variability depicted by the CEOFs in terms of boundary waves, we will use the results of Wise et al. (2020) derived from an idealised model. Following Wise et al. (2020), consider an idealised barotropic case of a western boundary, modelled by a rectangular domain with positive y in the direction of increasing latitude ($y = 0$ at the equator) and positive x in the direction of increasing longitude. The bottom topography is described by the function $h(x)$ and increases in depth monotonically from zero at the western edge (coast, $x = 0$) to some greater depth at the eastern edge of the domain, which is hundreds of kilometres east of the coast and is taken to be the interface between the western boundary region and the interior ocean. Note that while the bottom topography described by $h(x)$ is uniform alongshore, it does include a continental shelf and slope. The long-wave approximation momentum equations (Gill and Schumann, 1974), including a simple representation of alongshore dissipation via bottom friction, are

$$-fhv + gh\frac{\partial \tilde{\eta}}{\partial x} = 0, \tag{9}$$

$$h\frac{\partial v}{\partial t} + fhu + gh\frac{\partial \tilde{\eta}}{\partial y} = -rv, \tag{10}$$

where $\boldsymbol{u} = [u(x,y,t), v(x,y,t)]$ is the horizontal velocity, $\tilde{\eta}(x,y,t)$ is the dynamic sea level, g is gravity, $f = \beta y$ is the Coriolis parameter and r is the friction parameter. The continuity equation is given by $\nabla \cdot h\boldsymbol{u} = 0$. Assume that variability from the interior ocean occurs between a poleward latitude y_p and equatorward latitude y_e. In the interior ocean, variability on interannual time scales of basin scale can be carried westward by long Rossby waves and this can be represented by imposing a boundary condition on the eastern edge of the model domain in the form $\eta_{in}(y)e^{-i\omega t}$, where ω is the frequency of the variability and subscript *in* denotes interior. For variability with a multiannual or longer period, Wise et al. (2020) derive the solution in the form

$$\tilde{\eta}(x,y,t) = \eta(x,y)e^{-i\omega t}, \tag{11}$$

where

$$\eta(x,y) = \eta_{in}(y) - \int_{y}^{y_p} \sum_{j=1}^{\infty} W_j(x,y,s)\,ds. \tag{12}$$

Eqs. (11)–(12) show that the solution in the western boundary region consists of the long Rossby wave from the interior (first term on the right of (12)) modified by a second term, which captures the effect of the excited boundary waves, where W_j is complex and describes the boundary wave modes. Note that Marshall and Johnson (2013) derive a related solution for the first mode baroclinic case with a vertical sidewall (i.e. no continental shelf and slope). Eqs. (11) and (12) can be written in exponential form as

$$\tilde{\eta}(x,y,t) = A(x,y)e^{i[\varphi(x,y)-\omega t]}, \tag{13}$$

thus describing the response on the shelf and slope for a given frequency ω, by its amplitude A and phase φ. Note how this is in the same form as (8), which gives the variability described by each CEOF mode, hence each CEOF mode can be thought of in terms of (11) and (12), that is in terms of the long Rossby wave (the interior sea level variability just offshore of the slope) and the excited boundary waves that this variability generates.

A crucial point to note is that the effect of the boundary waves on the sea level at each latitude involves an integral of the waves between that latitude and the most poleward latitude of the variability. The sea level response on the continental shelf and slope at each latitude is therefore the combined effect of the long Rossby wave from the interior at that latitude and the sum of the boundary wave modes integrated over the latitudinal extent of the variability. It is in this way that variability from higher latitudes is able to affect the sea level response on the slope and shelf at lower latitudes, i.e. it propagates via the boundary waves. Note that Wise et al. (2020) showed that the effect of friction is to dampen the wave amplitudes as they propagate equatorward and dissipate energy. Hence regions of large dissipation reduce the extent to which boundary waves carry anomalies to lower latitudes.

As noted in the introduction, the drivers of coastal variability are debated because it is typically difficult to determine the pathways of variability from ocean-to-coast, i.e which sections of interior variability adjacent to the slope are driving sea level variability along specific sections of coastline. The phase and amplitude of the CEOFs in our simplified experiments are useful for determining this.

Figure panels 3d and 4d show the spatial phases of the CEOFs on the shelf in very fine colourmap resolution. The temporal phase of both modes of variability is positive, and in phase with the two wind forcing components. An approximate local wave number can be obtained from the spatial phase plots and the sign of the local wavenumber can be estimated by noting the direction of the phase lag. For example, decreasing spatial phase with increasing latitude implies a negative meridional wavenumber. Southward propagation on the shelf can be identified in both Figs. 3d and 4d. From theory, variability should be coherent in phase along the steepest parts of the topography, such as the slope, an idea supported by observations (Roussenov et al., 2008; Hughes and Meredith, 2006). This is difficult to see in our results due to the limited grid resolution on the upper slope, nevertheless it is clear from the Mean Pattern mode amplitude plot, Fig. 3b that while maximum interior variability (of the same phase as on the shelf) is located at 42N and 38N, the maximum amplitude on the shelf is at 33N and there is a distinct southward displacement of the inner-shelf amplitude relative to the outer-shelf.

The picture presented by the fine colourbar resolution plots in conjunction with Eqs. (11)–(13) is instructive and implies the CEOFs can be interpreted as follows. The interior SSH variability adjacent to the slope (the first term on the right in (12)) excites boundary waves which propagate equatorward (W_j in (12)). This southward propagation is evident in the phase plots on the shelf and slope (though propagation is not exclusively southward, which hints at possible nonlinear effects or effects of the local bathymetry not covered in idealised theory). The southward displacement in the amplitude of the variability on the shelf, clearly seen in the high resolution amplitude plots, is then the result of the integral of the boundary waves in (12) combined with the interior SSH. Hence hot spots of variability adjacent to the slope can drive variability on the shelf at lower latitudes.

Wise et al. (2020) showed that the boundary waves dissipate more of their energy and decay over a shorter distance when bottom friction is larger and where the bathymetry is steeper. Hence the degree of southward displacement of the interior variability as it penetrates onto the shelf, can depend on the local bathymetry and local dissipation (friction).

An appreciation of how the boundary wave mechanism adjusts coastal sea level is important. For example, when considering modulation of sea level south of Cape Hatteras, part of the variability will ultimately originate a number of degrees farther northward (in the interior and on-shelf). However, because the interior ocean signal may be correlated (i.e. the variability in the interior ocean may be coherent over many degrees of latitude) and because the boundary adjustment is rapid, it can be difficult to identify the northern origin of the variability. This point is clear when comparing the phase of the NAO Pattern mode in low resolution and high resolution.

Consider also the SSH variability in the Mean Pattern mode south of 33 N. On first inspection it appears as though the interior SSH variability offshore of the Florida coastline does not influence coastal SSH, however this is simply because the on-shelf and interior variability are in anti-phase, hence the interior variability in the Mean Pattern mode simply acts to reduce the amplitude of the on-shelf variability. At these latitudes the long wave and excited boundary waves (first and second terms on the right in (12)) nearly cancel one another.

The fine colourbar resolution amplitude and phase for the NAO Pattern mode, shown in Fig. 4b and d, again demonstrate the interior ocean signal appearing to leak onto the shelf at lower latitudes. The interior SSH signal offshore of Florida is now increasing (rather than decreasing) the amplitude of the on-shelf SSH variability because they are in phase. In this case the interior long wave and the excited boundary waves no longer cancel one another at those latitudes.

Furthermore, because trapped waves are sensitive to bottom topography (Wise et al., 2020; Huthnance, 1987), identifying signal origin could be particularly problematic when using coarse resolution models around areas such as the Florida straits, where bathymetric features can be difficult to resolve.

In a barotropic model the interior ocean adjusts quickly to variability in forcing (which is useful here), but in the real stratified interior ocean, baroclinic Rossby waves are slower, thus amplifying the decoupling in the timescale of response between the interior ocean and upper slope or shelf. For realistic damping and where changes in interior sea level occur over long time periods, the variability of forcing is slow relative to the adjustment at the boundary, and boundary waves effectively carry out the adjustment along the boundary instantaneously. In this case a reasonable approximation to (9) and (10) is to neglect time dependence giving a steady state form of the solution (11)–(12), i.e. equation (31) of Wise et al. (2020). This approach is adopted in idealised studies of western boundary sea level by Wise et al. (2018), Minobe et al. (2017) and Hong et al. (2000), producing good qualitative agreement with model output and observations. Therefore even for long period sea level change in the interior, it is instructive to see that there is a boundary wave contribution to the response along the boundary, but it is quick relative to the time scale of change in the interior.

To demonstrate this, we show in Fig. 7 the solution (12) in the steady state for three different interior sea level anomalies that correspond to the interior sea level anomalies produced by the Mean and NAO forcing Patterns in our numerical model experiments. We also show the long wave and boundary wave contributions to the solution (i.e. the two terms in the solution). Note that we used the solution derived in Wise et al. (2020) (their equation 31). The three experiments are detailed in Table 2. Panels 1(a–c) show the long wave contribution, the boundary wave contribution and their sum (the solution) for experiment 1 of Table 2. This experiment introduces an interior sea level anomaly representative of that created by the Mean Forcing Pattern (a change in the sea level associated with stronger subpolar and subtropical gyres). Panel 1a shows the interior sea level penetrate to the coast, panel 1b shows the adjustment term due to the excited boundary waves, and panel 1c shows the resulting net sea level response, where sea level change (here a decrease) in the subpolar gyre leaks onto the shelf with reduced magnitude and southward displacement (around Cape Hatteras). Further south of Cape Hatteras the influence of the subtropical gyre begins to cancel the effect of the subpolar gyre. The solution is highly consistent with the Mean Pattern CEOF in Figs. 3 and 5.

Panels 2(a–c) show the same for an interior sea level anomaly representative of that created by the NAO Forcing Pattern (an in-phase change in the interior sea level, experiment 2 in Table 2). The net response in panel 2c shows the interior sea level change (here an increase) leak onto the shelf south of Cape Hatteras. Again the sea level change magnitude is reduced and it is displaced southward relative to the interior. This is also highly consistent with the NAO Pattern CEOF in Fig. 4.

Table 2

Interior sea level anomaly η_{in} for three analytic model experiments. Here $\hat{y} = (y - y_{26})$ and $Y = (y_{46} - y_{26})$ where subscripts 26 and 46 indicate the latitude and where *overline* denotes the mean. $y = 0$ and $x = 0$ correspond to the equator and coast (where depth is zero) respectively. In all experiments the depth and distance of the shelf break and slope–interior interface from the coast are (200 m, 80 km) and (500 m, 85 km) respectively. In all experiments the friction parameter is $r = 0.001$ m/s and $\beta = 1.667 \times 10^{-11}$ s^{-1}. Note in all cases the sea level anomaly along the northern boundary equals the interior sea level at that latitude.

Experiment	η_{in} (m)
1	$\eta_{in} = 0.2\sin(2\pi\hat{y}/Y)$
2	$\eta_{in} = 0.2\sin(\pi\hat{y}/Y)$
3	$\eta_{in} = 0.2\sin(\pi\hat{y}/Y) - \overline{0.2\sin(\pi\hat{y}/Y)}$

The final experiment (3 in Table 2) is the same as the previous experiment (2), but by subtracting the mean over the domain from the interior anomaly we have introduced an anomaly along the northern boundary as well (this constant northern anomaly extends from the coast to the interior). This experiment is designed to represent the NAO Forcing Pattern in the case where the northern boundary was closed rather than radiative. Despite the change from experiment 2, panel 3b shows that the boundary wave response is in fact the same in the two cases, and the net response in panel 3c is different because we effectively added an anomaly across the entire domain (relative to experiment 2). This is clear since we could split panel 3a into its 2 linear terms; the first term is the same as in experiment 2 and the second is its mean, which is uniform across the domain. Panel 3c is as a result consistent with the NAO Pattern CEOF for the closed boundary in Fig. 6 showing that to the south, the interior signal will tend to cancel the northern sea level signal on the shelf.

A number of conclusions can be drawn from the consistency between the results of the idealised linear analytic model and the non-linear numerical model that uses more realistic bathymetry. Firstly, the conceptual framework, whereby the western boundary sea level responds to change in the interior sea level via the generation of rapid boundary waves that modify the influence of the interior sea level at the coast, appears to be robust. Secondly, this conceptual framework is instructive for explaining western boundary sea level change over interannual and longer time periods. Finally, because friction and bathymetry exert an influence over the decay characteristics of boundary waves (Wise et al., 2020; Huthnance, 2004), the modelling of boundary sea level can be sensitive to the representation of both in numerical models, e.g. changing the friction parameter changes the boundary wave contribution (panels (1-3)b in Fig. 7, which then changes the modelled sea level response (panels (1-3)c).

3.4. Non-linear effects

The extent to which nonlinear effects added by a mean flow, such as the Gulf Stream, will be important locally for the shelf and slope response to interior variability is an open question. It is possible for example that boundary wave propagation is significantly modified, which would modify how variability propagates along the shelf.

For the barotropic case, friction has previously been shown to play a dominant role in modifying boundary waves and determining the character of the response on the shelf. Specifically friction at the boundary results in dissipation and this has been shown in linear models to dampen boundary waves, enabling interior variability to leak onto the shelf (Wise et al., 2020; Marshall and Johnson, 2013; Huthnance, 2004, 1987). An important result from our non-linear barotropic model is that friction appears to remain a dominant process.

Neglecting horizontal diffusion, the role of friction in the barotropic vorticity equation can be related to the potential vorticity as

$$\frac{D}{Dt}\left(\frac{\zeta + f}{h}\right) = -\frac{1}{h}\nabla \times \left(\frac{\tau_b}{h}\right), \tag{14}$$
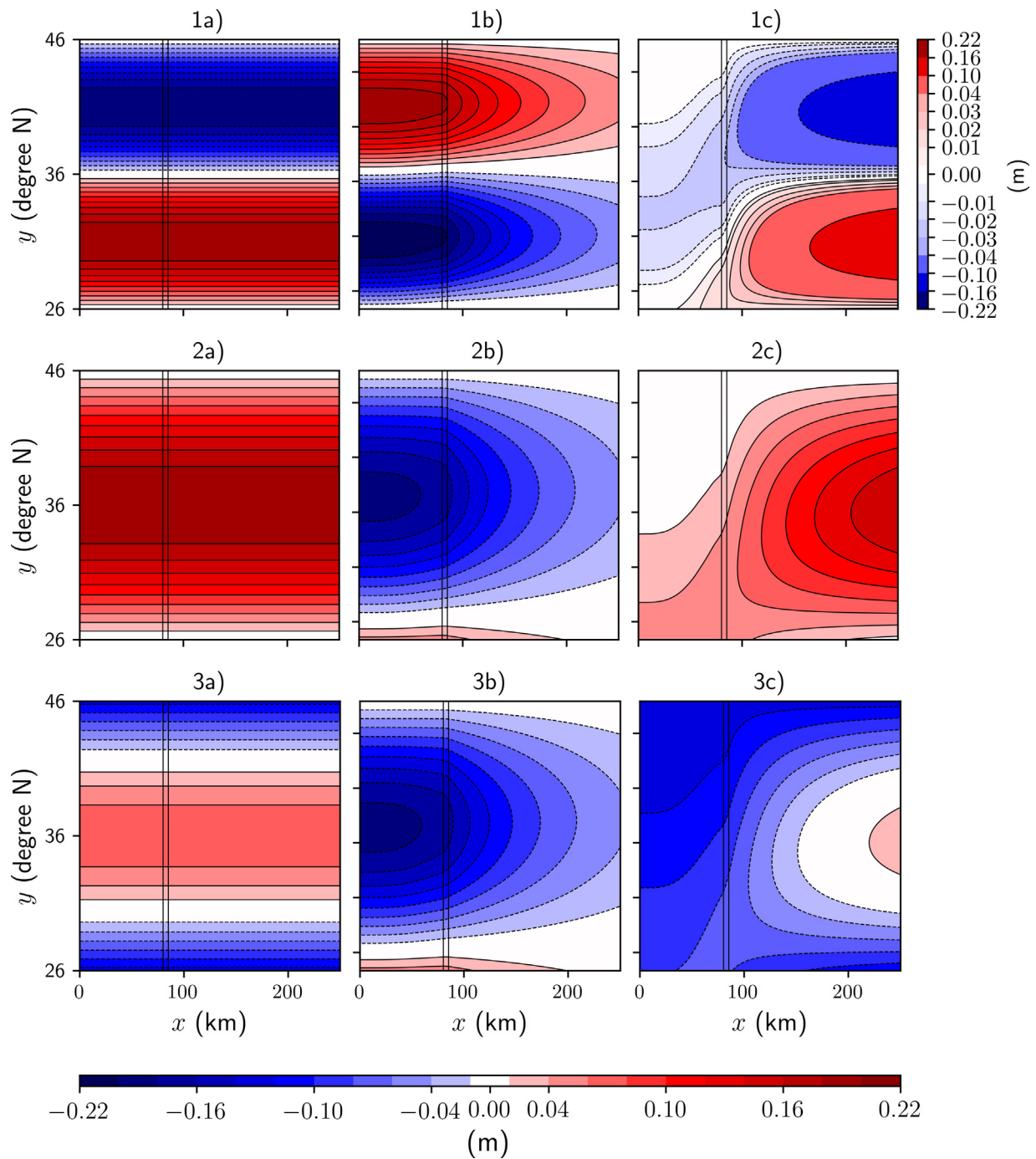
Fig. 7. Long wave contribution, boundary wave contribution and the solution (12) for the time independent version of the model described in Section 3.3, i.e. Eqs. (9) and (10), showing the sea level response along the western boundary to three different interior sea level anomalies, η_{in}. Each row corresponds to a different interior sea level anomaly. Rows 1, 2 and 3 correspond to experiments 1, 2 and 3 respectively in Table 2. Note that y is the alongshore and x is the cross-shore coordinate, with depth tending to zero at the coast $x = 0$. Each column shows a different term in (12): column (a) shows the long wave contribution from the interior (first term on right in (12)), column (b) shows the boundary wave contribution (second term on right in (12)) and column (c) shows the solution to (12) (sum of long and boundary wave contributions). The black lines indicate the shelf break ($x = 80$ km, depth 200 m) and where the upper slope and interior meet ($x = 85$ km, depth 500 m). Note that panel 1(c) has its own colourbar, which is non-uniform to provide greater detail.

where $D/Dt = \partial/\partial t + \boldsymbol{u} \cdot \boldsymbol{\nabla}$, $\boldsymbol{u}$ are horizontal velocities, $\boldsymbol{\nabla}$ is the horizontal derivative, f is the Coriolis parameter, h is the depth H plus free surface and $\boldsymbol{\tau}_b$ is bottom friction. Without friction, and with no mean flow ($\boldsymbol{u} = (u, v)$ are now anomalous velocities), potential vorticity ($\zeta + f)/h$ is conserved and the flow follows f/H contours (Salmon, 1998a). When the problem is framed in terms of dynamic sea level η, Wise et al. (2018) showed that it is natural to consider sea level contours following H/f contours (similarly for bottom pressure Salmon, 1998b). The inclusion of friction enables the flow to deviate and in the linear

case has been shown to enable sea level to penetrate from the interior onto the shelf, crossing H/f contours (Wise et al., 2018). The inclusion of a mean flow, clearly a consideration at western boundaries, will modify the background potential vorticity, for example $\zeta = \partial v/\partial x - \partial u/\partial y + V'(x)$, where V' is the shear of a meridional mean flow. As noted by Mysak (1980), when the shear is comparable to f, shelf waves can be significantly advected by the current. It is not clear however, to what extent this affects sea level penetration onto the shelf.
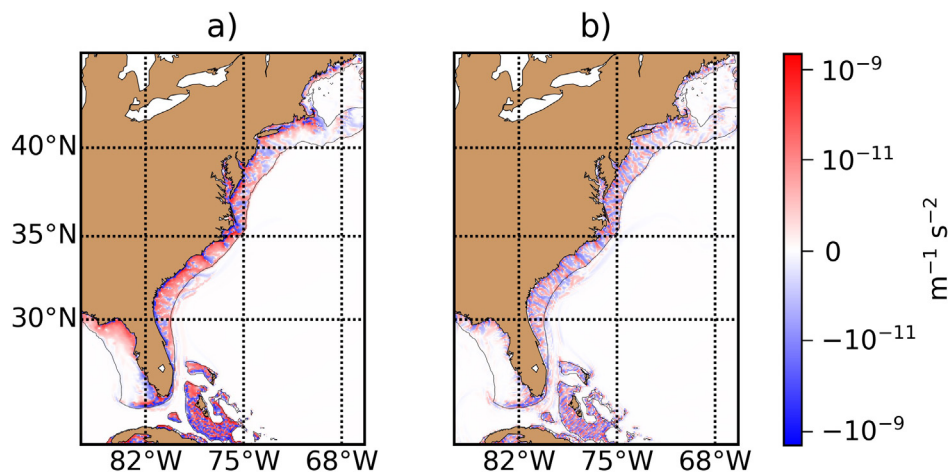
Fig. 8. Panel (a) shows the friction contribution to the time rate of change of the potential vorticity, i.e. right hand side of Eq. (14). (b) shows the non-linear contribution $\boldsymbol{u} \cdot \nabla(\zeta/h)$, where ζ is the relative vorticity and h the depth plus free surface. The black line denotes the 200 m depth contour.

For the case without fluctuating forcing, with the model in a quasi-steady state such that $\partial/\partial t \approx 0$, Fig. 8a shows the frictional contribution to (14), i.e. the term on the right. The figure shows a larger friction term on the slope and shelf and note also the enhanced off-shelf friction contribution between 31 N and 34 N where the upper slope widens and narrows, i.e. as the slope becomes narrow, friction increases — see Hill (1995) for a linear discussion of leakage due to a narrowing slope. Fig. 8b shows the non-linear relative vorticity contribution $\boldsymbol{u} \cdot \nabla(\zeta/h)$. While both terms are noisy, the important point is that the non-linear term is typically an order of magnitude smaller than the friction contribution. This suggests that even a strong mean flow does not significantly change the character of the frictional balance found in the linear case and therefore it does not prevent the low frequency on-shelf sea level being determined by the dynamics poleward of the point in question, i.e. the waves are not completely arrested by the mean current.

3.5. Stratification and other sources of variability

The consistency of the results with theory and observational studies is convincing. Nevertheless by assuming a barotropic ocean we have neglected certain processes that could modify our results. For example, Février et al. (2007) showed that variation in the thickness of the active subsurface layer of a 2.5 layer model as a result of Kelvin wave propagation, could induce a thickness anomaly in the upper layer. This forcing is proportional to the mean vorticity gradient and therefore can be large at the Gulf Stream separation area. This forcing on the upper layer does not prevent the Kelvin wave from propagating southward but does result in the appearance of a new coastal sea level anomaly with opposite sign in the vicinity of the Gulf Stream separation point. In addition, Dewar and Hogg (2010) and Deremble et al. (2017) discuss the role of non-viscous energy dissipation from the mesoscale at boundaries. They show that in a stratified flow, Kelvin and topographic waves trapped at the boundary can be "arrested" by an opposing balanced flow — potentially important along the US east coast where the Gulf Stream could arrest trapped boundary waves. It is worth speculating that the combined effects of stratification, topography and mean flow could, for example, be an alternative explanation for greater de-coherence between the regions north and south of Cape Hatteras than our results suggest.

Furthermore, it should be noted that the adjustment in the interior ocean will be slower and more latitude dependent in reality than in our model due to the fact that adjustment will take place via baroclinic Rossby waves rather than the faster barotropic Rossby waves (even in a 500 m depth layer). This implies that the temporal decoupling between deep ocean and coastal zone is more pronounced than our results

suggest — our results should be interpreted as the coastal response to the nearby ocean. Finally, the choice of a 500 m layer depth was chosen partly to generate a realistic Gulf Stream, however this will not be the best choice for all latitudes.

Early idealised models suggested that the coast is insulated from interior ocean variability by the steep continental slope (Wang, 1982; Csanady and Shaw, 1983). Our results and analysis add detail to this interpretation and show that the amplitude of interior variability is attenuated on the shelf. For both forcing patterns considered here, maximum interior variability is reduced in amplitude by approximately 80% on the shelf, giving for example centimetre order elevations for tens of centimetres anomalies in the interior. For comparison, changes in atmospheric pressure lead to similar order changes in sea level via the inverse barometer effect, where a 1 mbar decrease corresponds to a 1 cm increase in sea level. On-shelf wind stress is also a local driver of sea level change with order mm per year changes commonly resulting from interannual fluctuations (Domingues et al., 2018). Local inter-annual pressure and alongshore wind stress variability can therefore be important sources of centimetre scale sea level variability (Piecuch et al., 2019, 2016; Piecuch and Ponte, 2015). Another source of variability is the Sea Level Annual Cycle, which typically has an amplitude of centimetre order (Calafat et al., 2018). While these processes are important for setting the background sea level, which increases the likelihood of nuisance flooding, shorter time scale events such as storm surges due to hurricanes can act in addition to increased background sea level and can produce highly localised sea level anomalies measured in metres (Little et al., 2015). In this context it is clear that interior ocean variability is not the only relevant source of variability, nevertheless, it is clearly important to understand how large-scale changes in the oceans over many years might be communicated to the coast.

4. Summary

Observations have shown that sea level rise hot spots along the North American East Coast are correlated with a number of forcing phenomena and can appear at different latitudes. An understanding of the mechanisms by which the coast adjusts to forcing is important when explaining how hot spots of variability are distributed along the coast. Using a barotropic general circulation model of the North American East Coast that includes realistic coastal bathymetry and nonlinear terms, we have shown that there is good agreement with linear theory in modelling the coastal sea level response to SSH variability on the upper slope. Using a Hilbert transform Complex EOF method, we examine the propagation and amplitude of two modes of variability generated by interior ocean SSH anomalies that are characteristic of the remote SSH anomalies described by observational

studies. The Mean Forcing Pattern mode of variability describes in-phase variability along the entire coastline and is driven by a SSH anomaly in the subpolar gyre. The NAO Forcing Pattern mode of variability describes in-phase variability along the coast south of Cape Hatteras and is driven by an interior ocean SSH anomaly consistent with the NAO. Observations suggest that NAO-linked on-shelf wind and pressure forcing would drive an anomaly of opposite phase north of Cape Hatteras, though we have not tested this here. The results presented are shown to be consistent with linear barotropic trapped wave theory such that boundary waves propagate with the coast on the right, carrying SSH anomaly information equatorward along the shelf and slope. The role of boundary waves in the adjustment process is used to explain how coastal sea level variability can be sensitive to interior ocean variability many degrees of latitude further north, such that a hot spot of sea level variability in the subpolar gyre can drive a sea level anomaly to the north and south of Cape Hatteras. Indications from theory are that this southward displacement of variability is highly sensitive to the friction parameter on the shelf and slope (as well as local shelf width) (Wise et al., 2018, 2020) implying that an order of magnitude decrease in the friction parameter, for example, could increase the displacement further south of Cape Hatteras. The decay of topographic waves due to bottom friction, as described by linear theory, appears to be the key barotropic process determining the degree to which anomalies on the shelf are attenuated and displaced relative to the interior. This highlights the importance of accurately representing dissipation in numerical models. The inclusion of non-linear effects that enable advection of potential vorticity does not appear to significantly alter the dependence of coastal sea level on higher latitudes, and this ultimately suggests that the Gulf Stream does not stop the lower mode coastally trapped waves from propagating (acknowledging the limits of the barotropic assumption).

The analysis presented here fits in with the view that baroclinic variability might be strongly suppressed on western boundary shelves due to the rapid decay of higher wave modes as a result of the sloping topography and friction (Hughes et al., 2018). Furthermore, it better ties in coastal sea level variability with the growing theory of how anomalies propagate about ocean basins (e.g. Hughes et al., 2019; Marshall and Johnson, 2013; Johnson and Marshall, 2002; Clarke and Shi, 1991, and references therein) with relevance also for studies of the overturning circulation (Little et al., 2019).

CRediT authorship contribution statement

Declaration of competing interest

The authors declare that they have no known competing financial interests or personal relationships that could have appeared to influence the work reported in this paper.

Acknowledgements

References

Andres, M., Gawarkiewicz, G.G., Toole, J.M., 2013. Interannual sea level variability in the western North Atlantic: Regional forcing and remote response. Geophys. Res. Lett. 40 (22), 5915–5919.

Bingham, R.J., Hughes, C.W., 2009. Signature of the Atlantic Meridional Overturning Circulation in sea level along the East coast of North America. Geophys. Res. Lett. 36 (2).

Brink, K., 1991. Coastal-trapped waves and wind-driven currents over the continental shelf. Annu. Rev. Fluid Mech. 23 (1), 389–412.

Brink, K.H., Allen, J., 1978. On the effect of bottom friction on barotropic motion over the continental shelf. J. Phys. Oceanogr. 8 (5), 919–922.

Bryan, F.O., Hecht, M.W., Smith, R.D., 2007. Resolution convergence and sensitivity studies with North Atlantic circulation models. Part I: The Western boundary current system. Ocean Model. 16 (3–4), 141–159.

Calafat, F.M., Wahl, T., Lindsten, F., Williams, J., Frajka-Williams, E., 2018. Coherent modulation of the sea-level annual cycle in the United States by Atlantic Rossby waves. Nat. Commun. 9 (1), 2571.

Chapman, D.C., Brink, K.H., 1987. Shelf and slope circulation induced by fluctuating offshore forcing. J. Geophys. Res.: Oceans 92 (C11), 11741–11759.

Chassignet, E.P., Marshall, D.P., 2008. Gulf Stream separation in numerical ocean models. In: Geophysical Monograph Series, vol. 177, American Geophysical Union.

Clarke, A.J., Shi, C., 1991. Critical frequencies at ocean boundaries. J. Geophys. Res.: Oceans 96 (C6), 10731–10738.

Clarke, A.J., Van Gorder, S., 1994. On ENSO coastal currents and sea levels. J. Phys. Oceanogr. 24 (3), 661–680.

Csanady, G., Shaw, P.T., 1983. The "insulating" effect of a steep continental slope. J. Geophys. Res.: Oceans 88 (C12), 7519–7524.

Dengo, J., 1993. The problem of Gulf Stream separation: A barotropic approach. J. Phys. Oceanogr. 23 (10), 2182–2200.

Deremble, B., Johnson, E., Dewar, W., 2017. A coupled model of interior balanced and boundary flow. Ocean Model. 119, 1–12.

Dewar, W.K., Hogg, A.M., 2010. Topographic inviscid dissipation of balanced flow. Ocean Model. 32 (1–2), 1–13.

Domingues, R., Goni, G., Baringer, M., Volkov, D., 2018. What caused the accelerated sea level changes along the US East Coast during 2010–2015? Geophys. Res. Lett. 45 (24), 13–367.

Ezer, T., 2019. Regional differences in sea level rise between the Mid-Atlantic Bight and the South Atlantic Bight: Is the Gulf Stream to blame? Earth's Future 7 (7), 771–783.

Ezer, T., Atkinson, L.P., Corlett, W.B., Blanco, J.L., 2013. Gulf Stream's induced sea level rise and variability along the US mid-Atlantic coast. J. Geophys. Res.: Oceans 118 (2), 685–697.

Février, S., Sirven, J., Herbaut, C., 2007. Interaction of a coastal Kelvin wave with the mean state in the Gulf Stream separation area. J. Phys. Oceanogr. 37 (6), 1429–1444.

Flather, R.A., 1994. A storm surge prediction model for the northern Bay of Bengal with application to the cyclone disaster in April 1991. J. Phys. Oceanogr. 24 (1), 172–190.

Frederikse, T., Simon, K., Katsman, C.A., Riva, R., 2017. The sea-level budget along the Northwest Atlantic coast: GIA, mass changes, and large-scale ocean dynamics. J. Geophys. Res.: Oceans 122 (7), 5486–5501.

GEBCO Compilation Group, 2019. GEBCO 2019 grid. http://dx.doi.org/10.5285/836f016a-33be-6ddc-e053-6c86abc0788e.

Gill, A., Schumann, E., 1974. The generation of long shelf waves by the wind. J. Phys. Oceanogr. 4 (1), 83–90.

Gurvan Madec and NEMO System Team, 2019. NEMO ocean engine. http://dx.doi.org/10.5281/zenodo.1464816.

Hannachi, A., Jolliffe, I., Stephenson, D., 2007. Empirical orthogonal functions and related techniques in atmospheric science: A review. Int. J. Clim.: J. R. Meteorol. Soc. 27 (9), 1119–1152.

Hellerman, S., Rosenstein, M., 1983. Normal monthly wind stress over the world ocean with error estimates. J. Phys. Oceanogr. 13 (7), 1093–1104.

Hill, A.E., 1995. Leakage of barotropic slope currents onto the continental shelf. J. Phys. Oceanogr. 25 (7), 1617–1621.

Hong, B., Sturges, W., Clarke, A.J., 2000. Sea level on the US East Coast: decadal variability caused by open ocean wind-curl forcing. J. Phys. Oceanogr. 30 (8), 2088–2098.

Hughes, C.W., Fukumori, I., Griffies, S.M., Huthnance, J.M., Minobe, S., Spence, P., Thompson, K.R., Wise, A., 2019. Sea level and the role of coastal trapped waves in mediating the influence of the open ocean on the coast. Surv. Geophys. 40 (6), 1467–1492.

Hughes, C.W., Meredith, M.P., 2006. Coherent sea-level fluctuations along the global continental slope. Phil. Trans. R. Soc. A 364 (1841), 885–901.

Hughes, C.W., Williams, J., Blaker, A., Coward, A., Stepanov, V., 2018. A window on the deep ocean: the special value of ocean bottom pressure for monitoring the large-scale, deep-ocean circulation. Prog. Oceanogr. 161, 19–46.

Huthnance, J.M., 1975. On trapped waves over a continental shelf. J. Fluid Mech. 69 (4), 689–704.

Huthnance, J.M., 1978. On coastal trapped waves: Analysis and numerical calculation by inverse iteration. J. Phys. Oceanogr. 8 (1), 74–92.

Huthnance, J.M., 1987. Along-shelf evolution and sea levels across the continental slope. Cont. Shelf Res. 7 (8), 957–974.

Huthnance, J.M., 2004. Ocean-to-shelf signal transmission: A parameter study. J. Geophys. Res.: Oceans 109 (C12).

Huthnance, J., Mysak, L., Wang, D.-P., 1986. Coastal trapped waves. Baroclinic Process. Cont. shelves 3, 1–18.

Johnson, H.L., Marshall, D.P., 2002. A theory for the surface Atlantic response to thermohaline variability. J. Phys. Oceanogr. 32 (4), 1121–1132.

Kenigson, J.S., Han, W., Rajagopalan, B., Yanto, Jasinski, M., 2018. Decadal shift of NAO-linked interannual sea level variability along the US Northeast coast. J. Clim. 31 (13), 4981–4989.

Little, C.M., Horton, R.M., Kopp, R.E., Oppenheimer, M., Vecchi, G.A., Villarini, G., 2015. Joint projections of US East Coast sea level and storm surge. Nature Clim. Change 5 (12), 1114–1120.

Little, C.M., Hu, A., Hughes, C.W., McCarthy, G.D., Piecuch, C.G., Ponte, R.M., Thomas, M.D., 2019. The relationship between US East coast sea level and the Atlantic Meridional Overturning Circulation: A review. J. Geophys. Res.: Oceans 124 (9), 6435–6458.

Liu, Y., Wilson, C., Green, M.A., Hughes, C.W., 2018. Gulf Stream transport and mixing processes via coherent structure dynamics. J. Geophys. Res.: Oceans 123 (4), 3014–3037.

Marshall, D.P., Johnson, H.L., 2013. Propagation of meridional circulation anomalies along western and eastern boundaries. J. Phys. Oceanogr. 43 (12), 2699–2717.

Marshall, J., Johnson, H., Goodman, J., 2001. A study of the interaction of the North Atlantic Oscillation with ocean circulation. J. Clim. 14 (7), 1399–1421.

Minobe, S., Terada, M., Qiu, B., Schneider, N., 2017. Western boundary sea level: A theory, rule of thumb, and application to climate models. J. Phys. Oceanogr. 47 (5), 957–977.

Munday, D.R., Marshall, D.P., 2005. On the separation of a barotropic western boundary current from a cape. J. Phys. Oceanogr. 35 (10), 1726–1743.

Mysak, L.A., 1980. Topographically trapped waves. Annu. Rev. Fluid Mech. 12 (1), 45–76.

Park, J., Sweet, W., 2015. Accelerated sea level rise and Florida Current transport. Ocean Sci. 11 (4), 607–615.

Piecuch, C.G., Dangendorf, S., Gawarkiewicz, G.G., Little, C.M., Ponte, R.M., Yang, J., 2019. How is New England coastal sea level related to the Atlantic Meridional Overturning Circulation at 26 N? Geophys. Res. Lett. 46 (10), 5351–5360.

Piecuch, C.G., Dangendorf, S., Ponte, R.M., Marcos, M., 2016. Annual sea level changes on the North American northeast coast: Influence of local winds and barotropic motions. J. Clim. 29 (13), 4801–4816.

Piecuch, C.G., Ponte, R.M., 2015. Inverted barometer contributions to recent sea level changes along the northeast coast of North America. Geophys. Res. Lett. 42 (14), 5918–5925.

Polton, J.A., Wise, A., O'Neill, C.K., O'Dea, E., 2020. AMM7-Surge: A 7km resolution Atlantic Margin Model surge configuration using NEMOv3.6. http://dx.doi.org/10.5281/zenodo.4022310.

Roussenov, V.M., Williams, R.G., Hughes, C.W., Bingham, R.J., 2008. Boundary wave communication of bottom pressure and overturning changes for the North Atlantic. J. Geophys. Res.: Oceans 113 (C8).

Sallenger, Jr., A.H., Doran, K.S., Howd, P.A., 2012. Hotspot of accelerated sea-level rise on the Atlantic coast of North America. Nature Clim. Change 2 (12), 884–888.

Salmon, R., 1998a. Lectures on Geophysical Fluid Dynamics. Oxford University Press.

Salmon, R., 1998b. Linear ocean circulation theory with realistic bathymetry. J. Mar. Res. 56 (4), 833–884.

Valle-Levinson, A., Dutton, A., Martin, J.B., 2017. Spatial and temporal variability of sea level rise hot spots over the eastern United States. Geophys. Res. Lett. 44 (15), 7876–7882.

Volkov, D.L., Lee, S.-K., Domingues, R., Zhang, H., Goes, M., 2019. Interannual sea level variability along the southeastern seaboard of the United States in relation to the gyre-scale heat divergence in the North Atlantic. Geophys. Res. Lett. 46 (13), 7481–7490.

Wang, D.-P., 1982. Effects of continental slope on the mean shelf circulation. J. Phys. Oceanogr. 12 (12), 1524–1526.

Wise, A., Hughes, C.W., Polton, J.A., 2018. Bathymetric influence on the coastal sea level response to ocean gyres at western boundaries. J. Phys. Oceanogr. 48 (12), 2949–2964.

Wise, A., Hughes, C.W., Polton, J.A., Huthnance, J.M., 2020. Leaky Slope Waves and sea level: Unusual consequences of the beta effect along western boundaries with bottom topography and dissipation. J. Phys. Oceanogr. 50 (1), 217–237.

Zhai, X., Johnson, H.L., Marshall, D.P., 2011. A model of Atlantic heat content and sea level change in response to thermohaline forcing. J. Clim. 24 (21), 5619–5632.

Zhai, X., Johnson, H.L., Marshall, D.P., 2014. A simple model of the response of the Atlantic to the North Atlantic Oscillation. J. Clim. 27 (11), 4052–4069.